JOURNAL OF GEOPHYSICAL RESEARCH, VOL. 101, NO. D22, PAGES 28,753–28,767, DECEMBER 20, 1996

Past, present, and future modeled ozone trends with comparisons to observed trends

Charles H. Jackman,[1] Eric L. Fleming,[2] Sushil Chandra,[1] David B. Considine,[2] and Joan E. Rosenfield[3]

Abstract. The NASA Goddard Space Flight Center (GSFC) two-dimensional (2-D) model of stratospheric transport and photochemistry has been used to predict ozone changes that have occurred in the past 20 years from anthropogenic chlorine and bromine emissions, solar cycle ultraviolet flux variations, the changing sulfate aerosol abundance due to several volcanic eruptions including the major eruptions of El Chichón and Mount Pinatubo, solar proton events (SPEs), and galactic cosmic rays (GCRs). The same linear regression technique has been used to derive profile and total ozone trends from both measurements and the GSFC model. Derived 2-D model ozone profile trends are similar in shape to the Solar Backscattered Ultraviolet (SBUV) and SBUV/2 trends with highest percentage decreases in the upper stratosphere at the highest latitudes. The general magnitude of the derived 2-D model upper stratospheric negative ozone trend is larger than the trends derived from the observations, especially in the northern hemisphere. The derived 2-D model negative trend in the lower stratosphere at middle northern latitudes is less than the measured trend. The derived 2-D model total ozone trends are small in the tropics and larger at middle and high latitudes, a pattern that is very similar to the Total Ozone Mapping Spectrometer (TOMS) derived trends. The differences between the derived 2-D model and TOMS trends are generally within 1–2% in the northern hemisphere and the tropics. The derived 2-D model trends are generally more in southern middle and high latitudes by 2–4%. Our 2-D model predictions are also compared with the temporal variations in total ozone averaged between 65°S and 65°N over the TOMS observing period (1979–1993). Inclusion of anthropogenic chlorine and bromine increases, solar cycle ultraviolet flux variations, and the changing sulfate aerosol area abundance into our model captures much of the observed TOMS global total ozone changes. The model simulations predict a decrease in ozone of about 4% from 1979 to 1995 due to the chlorine and bromine increases. The changing sulfate aerosol abundances were computed to significantly affect ozone and result in a maximum decrease of about 2.8% in 1992 in the annually averaged almost global total ozone (AAGTO) computed between 65°S and 65°N. Solar ultraviolet flux variations are calculated to provide a moderate perturbation to the AAGTO over the solar cycle by a maximum of ±0.6% (about 1.2% from solar maximum to minimum). Effects from SPEs are relatively small, with a predicted maximum AAGTO decrease of 0.22% in 1990 after the extremely large events of October 1989. GCRs are computed to cause relatively minuscule variations of a maximum of +0.02% in AAGTO over a solar cycle.

1. Introduction

Stratospheric ozone has undergone significant decreases in the 1980s and early 1990s [e.g., *Stolarski et al.* 1991; *Bojkov et al.*, 1990; *Gleason et al.*, 1993; *Hofmann et al.*, 1994], and much of this ozone depletion is attributed to human activity [e.g., *World Meteorological Organization (WMO)*, 1991, 1995]. Natural variations also affect ozone and serve to either mitigate or enhance the decreases in ozone caused by increases in stratospheric chlorine and bromine. Examples of these natural atmospheric changes include (1) the solar cycle ultraviolet flux variation [e.g., *Garcia et al.*, 1984; *Huang and Brasseur*, 1993; *Fleming et al.*, 1995], (2) volcanic eruptions [e.g., *Brasseur and Granier*, 1992; *Tie et al.*, 1994; *Kinnison et al.*, 1994; *Solomon et al.*, 1996], (3) interannual temperature and dynamical changes [e.g., *Tung and Yang*, 1988; *Schneider et al.*, 1991; *Jackman et al.*, 1991a], (4) the quasi-biennial oscillation (QBO) [e.g., *Gray and Pyle*, 1989; *Gray and Dunkerton*, 1990], (5) downflux of NO_x (N, NO, NO_2, NO_3, and N_2O_5) from the thermosphere [e.g., *Garcia et al.*, 1984; *Solomon and Garcia*, 1984; *Siskind and Russell*, 1996], (6) solar proton events (SPEs) [e.g., *Jackman et al.* 1990, 1995a, b; *Reid et al.*, 1991], (7) galactic cosmic rays (GCRs) [e.g., *Legrand et al.*, 1989; *Jackman*, 1993; *Jackman et al.*, 1995b], and (8) relativistic electron precipitations [e.g., *Thorne*, 1977; *Callis et al.*, 1991].

Since two-dimensional (2-D) models are employed to help assess the long-term effect of anthropogenic halocarbons on stratospheric ozone [*WMO*, 1991, 1995], it is useful to investi-

[1]Laboratory for Atmospheres, NASA Goddard Space Flight Center, Greenbelt, Maryland.
[2]Applied Research Corporation, Landover, Maryland.
[3]General Sciences Corporation, Laurel, Maryland.

Paper number 96JD03088.
0148-0227/96/96JD-03088$09.00

gate the ability of such models to predict ozone variabilities and trends that have been observed. Some problems with model predictions of total ozone trends have been discussed in the *WMO* [1995] report. The modeled trends are generally consistent with or slightly larger than the lower latitude trends derived from Total Ozone Mapping Spectrometer (TOMS) version 6 measurements. However, the modeled trends tend to be smaller than the derived ozone trends at middle and high latitudes.

Five recent occurrences have motivated us to reexamine modeled versus derived ozone trends:

1. The TOMS data have recently undergone a full reprocessing with the use of a new algorithm [*McPeters et al.*, 1996a, b; *McPeters and Labow*, 1996]. The "new" version 7 TOMS data show some differences when compared to the version 6 TOMS data, both in absolute values and in derived trends.
2. Ultraviolet (UV) solar fluxes have now been measured by instruments aboard the Upper Atmosphere Research Satellite (UARS) between solar maximum (fall 1991) and near–solar minimum (fall 1995) conditions. These UV data, along with ground-based 10.7-cm flux ($F10.7$) measurements, provide an opportunity to derive a relationship between UV solar flux changes and 10.7-cm flux changes [*Chandra et al.*, 1995b]. This analysis makes it possible to use the 10.7-cm flux variations which are available since 1947 as a transfer standard to derive the long-term UV solar flux changes for non-UARS observing years.
3. Extinction measurements by Stratospheric Aerosol and Gas Experiment (SAGE) I and II, Stratospheric Aerosol Measurement (SAM) II, and Solar Mesosphere Explorer (SME) can be used to derive stratospheric sulfate aerosol (SSA) layer surface area density distributions for the time period 1979–1995. *Solomon et al.* [1996] calculated ozone trends in the northern midlatitudes from 1979 to 1995 using variations in sulfate aerosol surface area densities calculated from satellite observations. They found that the model agreement with observations was significantly increased using the observed SSA variability. They also speculated that some fraction of the ozone trend resulting from SSA variations could be mistakenly attributed to solar UV variability. Separate analyses of the SSA and solar UV effects on ozone are needed to help quantify the interplay of these two natural variations.
4. The influence of solar proton events and galactic cosmic rays on odd nitrogen over the period 1974–1993 were derived by *Vitt and Jackman* [1996]. The solar proton fluxes were taken from Interplanetary Monitoring Platform (IMP) 8 measurements, and the galactic cosmic ray fluxes were scaled using sunspot number measurements.
5. Our 2-D model has undergone significant changes in the past 2 years. The model's photolysis rates and transport have been improved, and both are discussed in this paper. The revised model photolysis rates agree better with the photolysis benchmark created for models in the work leading up to the "1995 Scientific Assessment of the Atmospheric Effects of Stratospheric Aircraft" [*Stolarski et al.*, 1995]. The new model transport algorithm creates greater tropical isolation, creates greater polar isolation during winter, and also shows the subtropical-midlatitude "surf zone," all in better agreement with long-lived tracer measurements.

We have undertaken this study because of the aforementioned five recent developments. In this 2-D model study we will include the anthropogenic halocarbon emissions and the natural variations of the ultraviolet solar flux, the stratospheric sulfate aerosol surface area, solar proton fluxes, and galactic cosmic rays. The influence of each of these five variations on ozone will be discussed and quantified.

2. Model Description

Before the discovery of the "Antarctic ozone hole" in 1985, heterogeneous processes occurring on the surfaces of lower stratospheric aerosol particles were thought to play a minor role in lower stratospheric photochemistry. These processes were therefore neglected in the two-dimensional atmospheric models developed in the 1970s and early 1980s. Now that the central role played by heterogeneous reactions is recognized, practically all 2-D models include heterogeneous reactions on the background sulfate aerosol layer [*Prather and Remsberg*, 1993], and many of them include a method of incorporating heterogeneous reactions on polar stratospheric clouds [e.g., *Pitari et al.*, 1993; *Considine et al.*, 1994; *De Rudder et al.*, 1996]. The ability of models to predict long-term trends in ozone has improved dramatically with the introduction of these heterogeneous processes [e.g., *WMO*, 1991, 1995]. The calculation of dynamics in some 2-D models has also undergone substantial changes in the past several years. *Garcia et al.* [1992] and *Bacmeister et al.* [1995] showed that treatments of planetary and gravity waves in a zonal-mean model can enhance the polar vortex isolation and influence the overall residual circulation in a 2-D model.

The 2-D model at NASA Goddard Space Flight Center (GSFC) has also undergone much development over the past several years. The model was first described by *Douglass et al.* [1989]. Its altitude range was extended through the mesosphere by *Jackman et al.* [1990]. Heterogeneous processes occurring on the stratospheric sulfate aerosol layer and on polar stratospheric clouds (PSCs) are included in the manner described by *Considine et al.* [1994]. Heterogeneous reaction rates for $ClONO_2$ on the SSA layer are calculated following *Hanson and Ravishankara* [1994]. Heterogeneous reactions on PSCs composed of nitric acid trihydrate have been adjusted to account for the local relative humidity as suggested by *Tabazadeh and Turco* [1993] and *Hanson and Ravishankara* [1993]. Reaction rates and photolysis cross sections in the model have been updated to the Jet Propulsion Laboratory (JPL) recommendation [*DeMore et al.*, 1994]. We also include CH_4 photolysis cross sections from *Turco* [1975].

A look-up table is now used for the photolytic source term (PST) and photolysis of O_2 [$J(O_2)$]. This table was generated by R. Kawa (GSFC) using a radiation code developed by D. Anderson and coworkers at the Johns Hopkins University Applied Physics Laboratory [*Anderson and Meier*, 1979; *Anderson and Lloyd*, 1990]. The PST and $J(O_2)$ table is a function of wavelength, solar zenith angle, and column ozone and is given on the pressure grid of the GSFC 2-D model. The PST is computed for the particular wavelength, solar zenith angle, column ozone, and pressure of interest and is multiplied by the solar irradiance at the top of the model to compute the reduced (or enhanced) flux at the point of interest. The reduced (or enhanced) flux is then used with the photodissociation cross section for a particular constituent to derive the photolysis rate of interest.

The model transport algorithm has also recently been modified and is significantly different from that used previously [see *Jackman et al.*, 1991b; *Fleming et al.*, 1995]. The new algorithm will be discussed in detail in a forthcoming paper and is briefly

described here. The methodology generally follows that of other "coupled" two-dimensional models [e.g., *Garcia et al.*, 1992; *Bacmeister et al.*, 1995], as originally formulated by *Garcia and Solomon* [1983]. However, in order to maintain the climatological character of the model, the new transport fields are based on empirical data sets, as opposed to being computed interactively in the model. A meridional stream function is calculated to obtain the transformed Eulerian circulation ($\bar{v}^*$, $\bar{w}^*$). The coefficients of the elliptic stream function equation depend on the zonal mean temperature and zonal wind, which are based on the 17-year average (1979–1995) of temperature data from the National Centers for Environmental Prediction (NCEP), formerly known as the National Meteorological Center, for 1000–1 mbar, and the CIRA (1986) empirical reference model for the mesosphere above 1 mbar [*Fleming et al.*, 1990]. Zonal wind is derived from temperature using the gradient wind relation.

Forcing of the stream function is proportional to the vertical gradient of the mechanical forcing from planetary waves (X_p), gravity waves (X_g), and equatorial Kelvin waves (X_k) and the latitudinal gradient of the total heating rate. We have computed diabatic heating rates following *Rosenfield et al.* [1994], utilizing climatological distributions of temperature, ozone, and water vapor. The climatological latent heating rate distribution is adapted from *Newell et al.* [1974]. Forcing from planetary waves (X_p) is proportional to the Eliassen-Palm (E-P) flux divergence [e.g., *Andrews et al.*, 1987], which we have computed offline from the 17-year NCEP three-dimensional analyses for 1000–1 mbar and from the CIRA (1986) planetary wave climatology [*Barnett and Labitzke*, 1990] for the mesosphere above 1 mbar. Following *Randel and Garcia* [1994], latitudinal eddy diffusion (K_{yy}) is then obtained self-consistently as the ratio of the E-P flux divergence to the latitudinal gradient of zonal mean potential vorticity. To obtain distributions of vertical eddy diffusion (K_{zz}) and mechanical forcing from gravity waves (X_g), we have incorporated into the model the parameterization originally developed by *Lindzen* [1981] and modified by *Holton and Zhu* [1984]. Here we utilize the empirical zonal mean temperature and zonal wind fields (described above) in the parameterization to diagnose the latitudinal, seasonal, and vertical distributions of gravity wave drag X_g and diffusion based on a given set of gravity wave parameters. To approximate the circulation associated with the equatorial semiannual oscillation (SAO), we use the methodology of *Dunkerton* [1979] and *Gray and Pyle* [1987] along with the empirical zonal mean wind field to diagnose the mechanical forcing X_k from thermally damped equatorial Kelvin waves.

We have also implemented a new numerical advection scheme based on *Lin and Rood* [1996], which utilizes the piecewise parabolic method (PPM) [e.g., *Colella and Woodward*, 1984; *Carpenter et al.*, 1990]. This replaces our previous scheme based on *Prather* [1986]. The PPM is highly accurate and has the advantage of preserving sharp tracer gradients quite well. Comparisons between long-lived tracer distributions calculated with this new transport algorithm and observations are discussed below to show that the new algorithm adequately represents zonal mean transport processes in the atmosphere.

3. Halogen Increases

Over the past 2 decades, models have been used to help understand the influences of anthropogenic halocarbons (e.g., $CFCl_3$, CF_2Cl_2, CCl_4, $C_2Cl_3F_3$, $C_2Cl_2F_4$, C_2ClF_5, CH_3CCl_3, $CHClF_2$, $CBrClF_2$, $CBrF_3$, CH_3Br) on stratospheric ozone. Many measurements show the growth with time of halocarbons in the atmosphere [e.g., *Elkins et al.*, 1993; *Cunnold et al.*, 1994; *Kaye et al.*, 1994; *Montzka et al.*, 1996]. The UARS Cryogenic Limb Array Etalon Spectrometer (CLAES) provided good measurements of halocarbon CF_2Cl_2 (CFC-12) on a nearly global scale for about 19 months [*Kumer et al.*, 1993; *Nightingale et al.*, 1996]. Plate 1 (top) shows a zonal mean representation of monthly averaged CLAES measurements for September 1992.

Plate 1 (bottom) shows the model-calculated CF_2Cl_2 distribution for September 1992, which can be compared with the CLAES CF_2Cl_2 retrieval. The model distribution was obtained from a time-dependent model run from 1970 through 1995, with varying source gases, solar cycle ultraviolet flux, stratospheric sulfate aerosol, solar proton flux, and galactic cosmic ray flux. These contributions to atmospheric variability are discussed in sections 5.1, 5.2, 5.3, 5.4, and 5.5, respectively. We designate this model calculation as our "standard" simulation. The comparison includes only the region of the atmosphere covered by CLAES. In general, the comparison indicates that the model qualitatively reproduces the transport of source gases from the ground to the stratosphere. The new model transport algorithm does a satisfactory job of reproducing the characteristic dynamical features observed in this long-lived tracer. These include strong descent in the late winter polar vortex down to levels below 10 mbar with large horizontal gradients across the vortex edge near 60°S, relatively weak latitudinal gradients at 20°–50°S associated with the subtropical winter hemispheric "surf zone," and sharper gradients near 15°S associated with weak horizontal mixing between the winter subtropics and tropics. Both measurements and the model simulation also show the tropical bulge of CF_2Cl_2 toward the northern hemisphere. The measurements do indicate a generally stronger downward motion at the higher latitudes of both hemispheres below 20 mbar than is represented in the model and sharper horizontal gradients at the winter vortex and tropical boundaries. Although there still are model-measurement disagreements, this new circulation significantly improves the zonal mean representation of long-lived tracers compared with previous versions of the model.

The various halocarbon source gases produce inorganic halogen compounds through interaction with ultraviolet light, $O(^1D)$, and OH. These products of the organic halogen source gases have also been measured in the atmosphere. The two most dominant constituents of the inorganic fluorine and chlorine families are HF and HCl, respectively. At 55 km our 2-D model predicts that HF and HCl account for about 95% of their respective inorganic halogen families.

Our model computed HF is compared to the UARS Halogen Occultation Experiment (HALOE) observations [*Russell et al.*, 1993, 1996a; *Luo et al.*, 1994] in Plate 2 for September–October 1992. The model does a very reasonable job of predicting the qualitative and quantitative behavior of HF, suggesting that the breakdown of fluorine-containing source gases is well simulated. HF and CF_2Cl_2 are inversely correlated, as HF increases with altitude and CF_2Cl_2 decreases with altitude. This relationship is expected because CF_2Cl_2 is one of the primary sources of HF. Note also that many of the dynamical features apparent in Plate 1 are prominent in Plate 2, including the tropical bulge, the subtropical-midlatitude surf zone, and the strong downward descent at polar latitudes. The HF mea-

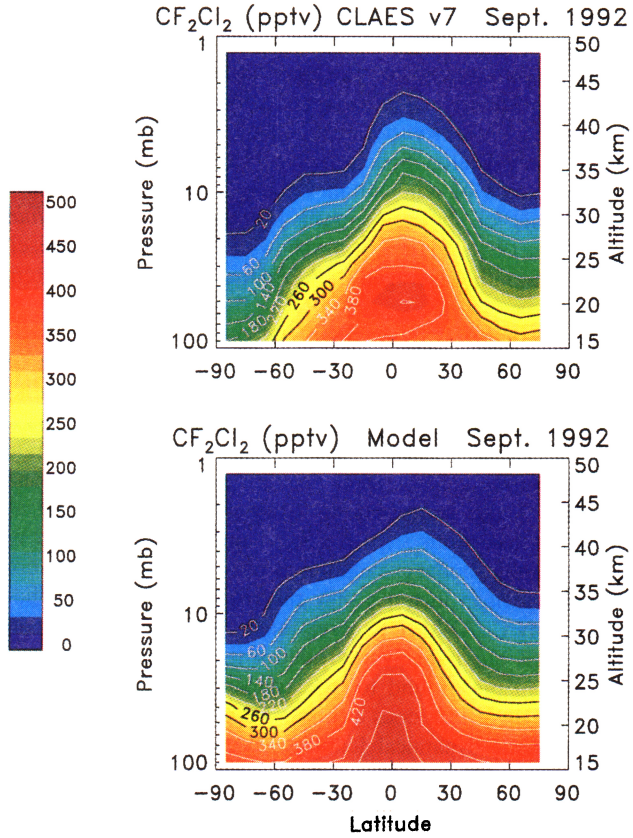

Plate 1. Zonal average CF_2Cl_2 for September 1992 from (top) UARS CLAES version 7 measurements and (bottom) the GSFC 2-D model.

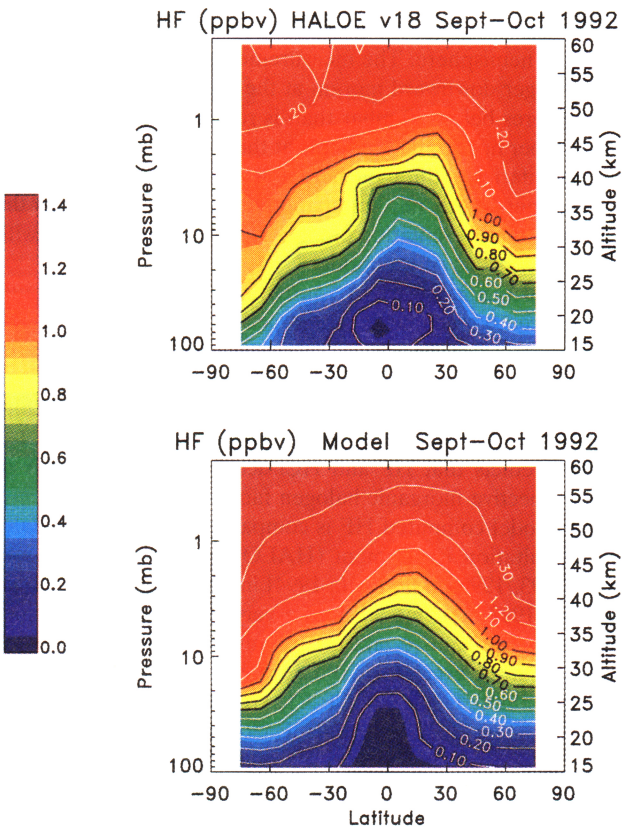

Plate 2. Zonal average HF for September–October 1992 from (top) UARS HALOE version 18 measurements and (bottom) the GSFC 2-D model.

surements also indicate a double-peaked structure about the equator in the upper stratosphere induced by the SAO meridional circulation during the equinoxes. This feature is much more evident in our model simulation for April (not shown) compared to September–October (Plate 2). Although the SAO circulation in the model is underestimated during September–October, the seasonal asymmetry of the model circulation is qualitatively similar to observations in which the double-peaked structure is somewhat stronger during the first (April) cycle of the year [e.g., *Randel et al.*, 1994; *Delisi and Dunkerton*, 1988].

Both the Atmospheric Trace Molecule Spectroscopy (ATMOS) experiment [*Zander et al.*, 1990; *Gunson et al.*, 1994] and HALOE [*Russell et al.*, 1996a, b] show increasing trends in global average HF and HCl at 55 km, as shown in Figure 1. The ATMOS measurements (represented by "squares") and the HALOE measurements (represented by dots) show some differences in the increasing trends for HF. Both sets of measurements show similar increasing trends in HCl although the ATMOS measurements are, on average, about 10–15% higher than the HALOE measurements. It is likely that there is a small seasonal variation bias in the ATMOS measurements, since these data were taken at different times of the year. However, this bias is not expected to change the overall result in Figure 1.

Our standard simulation gives yearly global average values represented by the solid lines in Figure 1. The trend simulated

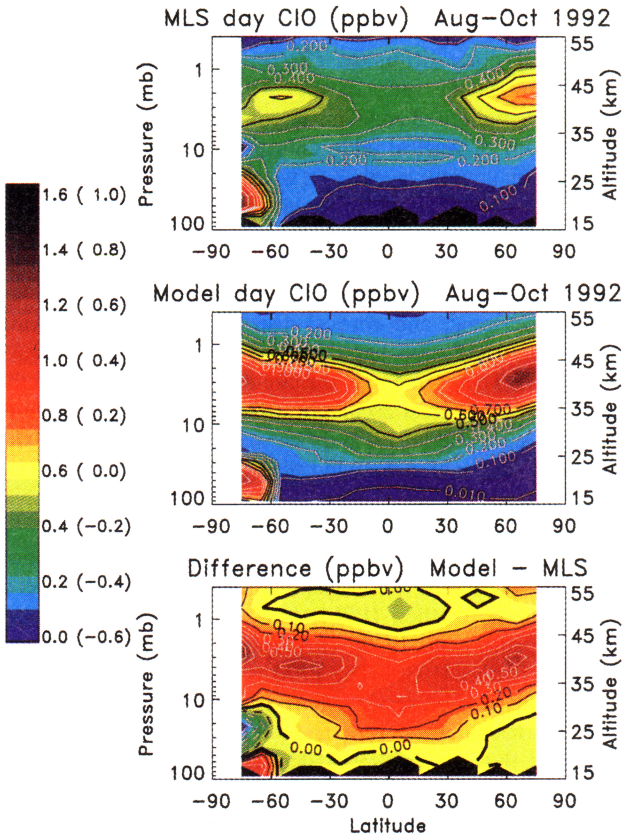

Plate 3. Zonal average ClO for August–October 1992 from (top) UARS MLS version 3 measurements, (middle) the GSFC 2-D model, and (bottom) the difference between model and measurements. The scale on the color bar is in parts per billion by volume (ppbv), and the difference in ppbv is in parentheses.

by the model for HF is somewhat different from that measured by ATMOS and slightly different from that observed in HALOE. The model simulation of HF shows little, if any, systematic bias in absolute value compared to both the ATMOS and HALOE measurements. The model-simulated HCl trend is similar to that measured by ATMOS and is slightly different from that measured by HALOE. The model HCl is systematically lower than ATMOS measurements (generally <5%) and higher than HALOE measurements (generally <10%).

The model predicts a leveling off in the accumulation of halogens in the atmosphere during the time period 1994–1996, while the HALOE measurements show a more constant increase in halogens over the same period. Minor deficiencies in the time-dependent halogen source gas boundary conditions, large-scale transport, loss rates of halogen source gases, and/or other aspects of the model simulation could all contribute to these model-measurement disagreements.

Another important inorganic halogen constituent, ClO, is shown in Plate 3. The UARS Microwave Limb Sounder (MLS) measurements [e.g., *Waters et al.*, 1996] for the time period August–October 1992 are shown (top) along with our 2-D model predictions (middle) and the difference between the model and MLS measurements (bottom). The model appears to do a reasonable job of activating chlorine in the Antarctic lower stratosphere, although it predicts substantially more ClO than measured in the middle and upper stratosphere. This historical model problem has been addressed before [e.g., *Chandra et al.*, 1993, and references therein] but has yet to be resolved satisfactorily.

The above comparisons suggest that the 2-D model transports and breaks down halocarbon source gases in the atmosphere reasonably correctly. However, there are some problems in simulating ClO, which have significant influence on the ability of our model to simulate ozone.

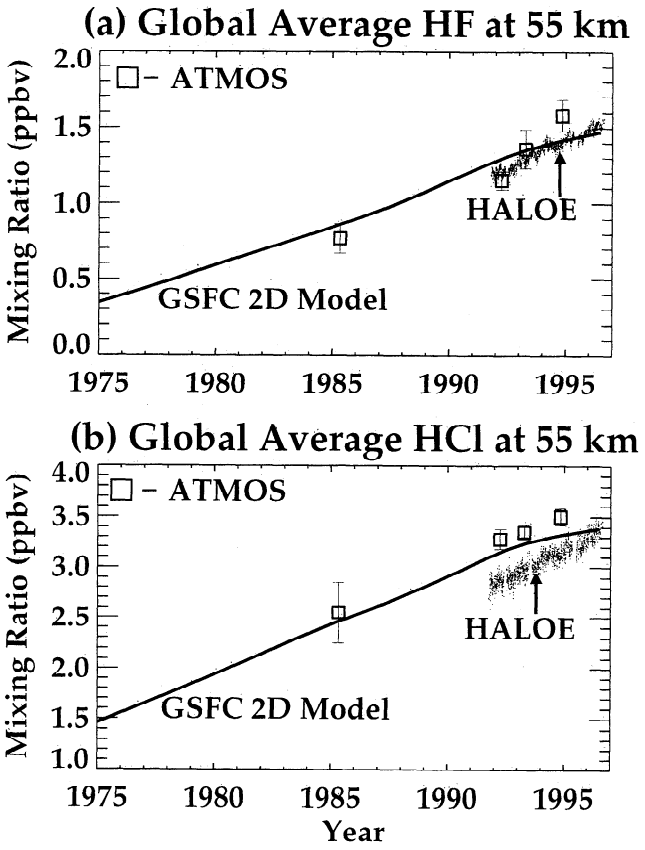

Figure 1. Global average values for (a) HF and (b) HCl from ATMOS (represented by squares), UARS HALOE version 18 (dots), and the GSFC 2-D model (solid lines). ATMOS measurements were in 1985, 1992, 1993, and 1994.

4. Ozone Trends

4.1. Profile Ozone Trends

We show a comparison of our model output for ozone compared with NOAA 11 Solar Backscattered Ultraviolet 2 (SBUV/2) measurements [e.g., *Planet et al.*, 1996] in September 1992 in Plate 4. The measurements (top) and model computations (middle) are shown along with the percentage difference of model minus measurements (bottom). Note that our model predicts ozone to within about 20% of that measured for all altitudes and latitudes presented. The model shows the well-known ozone deficit problem [e.g., *Minschwaner et al.*, 1993; *Eluszkiewicz and Allen*, 1993; *Dessler et al.*, 1996] in the tropical upper stratosphere, where model-calculated ozone can be up to 15% lower than that measured. We have found that this ozone deficit problem in our model is directly related to the overprediction of ClO, noted in the preceding section. In the middle stratosphere near 10 mbar the model predicts too much ozone. This feature, which is unrelated to the overprediction of ClO, is due in part to a "self-healing" process of ozone. The "self-healing" is caused by the deficit of ozone in the upper stratosphere allowing a larger flux of solar UV to lower altitudes, some of which is capable of photolyzing O_2 and producing ozone [e.g., *Jackman and McPeters*, 1985, and references therein]. However, in general, the agreement between modeled and measured ozone is fairly good.

We have previously presented a comparison of annually averaged profile ozone trends from 1979 to 1993 [*Chandra et al.* [1995a, Figure 1]. We now use a linear regression model to derive ozone trends from our 2-D model output as well as SBUV and SBUV/2 measurements (see Figure 2). The linear regression model consisted of the seasonal cycle, linear trend, quasi-biennial oscillation, and 11-year solar cycle as discussed in a number of papers [e.g., *Hollandsworth et al.*, 1995]. As in the *Chandra et al.* [1995a] study, the comparison of the derived 2-D model and observed trends shows some similarity in the latitude and altitude characteristics. Both the 2-D model and data show a maximum percentage decrease in the upper stratosphere–lower mesosphere at high latitudes. The derived 2-D model trends are still larger than those derived from observations in the northern hemisphere upper stratosphere. For example, near 50°–60°N and between 3 and 1 mbar (40–45 km) the derived 2-D model trends are just over −12%, whereas the measurements indicate trends just over −6%. The derived 2-D model ozone trend is also approximately symmetric about the equator, whereas the measurements show a significant asymmetry with larger negative trends at higher altitudes in the southern middle and high latitudes compared to the northern latitudes. The derived 2-D model trends are reasonably similar to the derived observed trends of −8% to −10% in the southern hemisphere upper stratosphere near 50°–60°S. The shaded areas in the derived SBUV and SBUV/2 profile ozone trends indicate regions where there is no statistically significant trend.

We compare the derived 2-D model ozone trends for the 1980s with those measured by four different instrumentation systems in Figure 3 for the 30°–50°N latitude band. The measurements of SBUV, SAGE I and II, Umkehr, and the ozone sondes are represented by the symbols (all taken from *WMO*

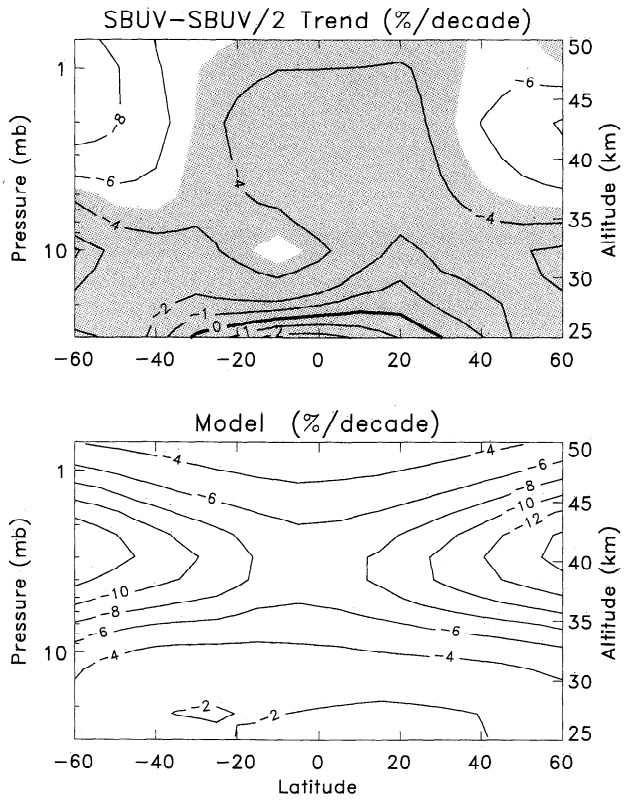

Figure 2. Zonally averaged derived ozone trends from 1979 to 1993 from (top) SBUV and SBUV/2 measurements and (bottom) the GSFC 2-D model. The trends were derived using a linear regression technique described in the text. The shaded areas in the derived SBUV and SBUV/2 trends indicate regions where there is no statistically significant trend.

[1995, Figure 1-14], and the derived 2-D model trends are represented by the dark solid line. The four measurements show some differences. For example, in the upper stratosphere the Umkehr, SAGE I and II, and SBUV show derived peak negative ozone trends between 35 and 40 km, near 40 km, and between 40 and 45 km, respectively. Between 15 and 25 km in the lower stratosphere, the sonde derived trend is between −2 and −7%/decade, while the SAGE I and II derived trend is between −2 and −20%/decade. The derived 2-D model trend peaks between 40 and 45 km at almost −12%/decade, whereas the measurements indicate trends between −5 and −8%/decade in that altitude range. In the lower stratosphere the derived 2-D model trends are generally lower than the trends derived from the sonde measurements and substantially lower than the trends derived from SAGE measurements in the region 15–20 km. The derived trends from the 2-D model, sondes, and SAGE all show increasing negative values with decreasing altitude below 25 km, although each trend has a different slope. We have discussed here and in previous works [*Chandra et al.*, 1993, 1995a] that there are some problems in the upper stratosphere with model-computed ozone and ClO. Computed ozone is low in comparison with measurements, and ClO is high. If adjustments are made to the model, such as adding the $ClO + OH \rightarrow HCl + O_2$ reaction at a 7% branching ratio, then the computed ozone and ClO are in better agreement with measurements, and the computed ozone trends are also reduced (from about −12 to −9%/decade). However, since we use the JPL recommendations [*DeMore et al.*, 1994] for reaction rates in these standard model simulations, the $ClO + OH \rightarrow HCl + O_2$ reaction is not included.

4.2. Total Ozone Trends

Ozone measurements from the Nimbus 7 TOMS instrument, which operated from November 1978 to May 1993, have

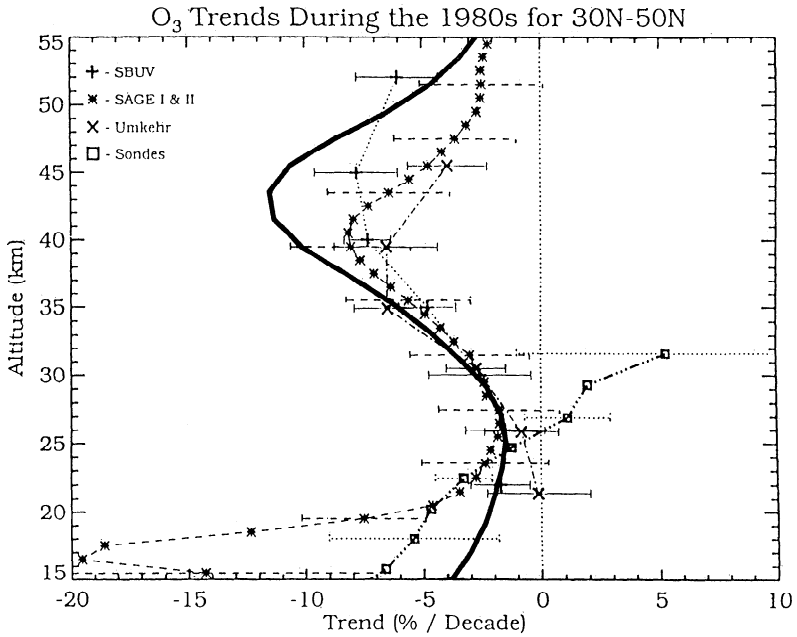

Figure 3. Zonally averaged derived ozone trends for the 1980s in the latitude band 30°–50°N from SBUV (plus signs), SAGE I and II (stars), Umkehr (crosses), sondes (squares), and the GSFC 2-D model (solid line). The measurement values were all taken from *WMO* [1995, Figure 1-14].

been extended through December 1994 using data from the second TOMS instrument onboard the Russian Meteor 3 satellite. Both these data sets have been recently recalibrated and reprocessed using the version 7 retrieval algorithm [*McPeters et al.*, 1996]. Our standard model total ozone simulation (averaged over 1988–1992) is shown in Plate 5 (middle), along with the newly reprocessed version 7 TOMS data (top), also averaged over 1988–1992, and the difference between the model and measurements (bottom). Much of the structure apparent in the measurements is captured in the model simulation, including (1) the on-the-pole maximum in the northern late winter–early spring, (2) the tropical low ozone levels and tropical seasonal structure, (3) the off-the-pole maximum in the southern late winter–spring, and (4) the very low ozone on the southern pole characterizing the Antarctic ozone hole in the spring. There are some differences in the model total ozone simulation: (1) the model predicts larger amounts of ozone for the middle latitude summer and early fall in both hemispheres, (2) the computed southern off-the-pole maximum is more equatorward and occurs at a slightly earlier time than the observed maximum, and (3) the breakup of the southern hemisphere polar low-ozone region in spring and the well-mixed region between the midlatitudes and the pole during December–January seen in the TOMS data is weakly represented in the model. In general, there is reasonable agreement between our model and measurements.

Figure 4 shows the TOMS version 7 derived trend (Figure 4a) based on 14 years of data from January 1979 through December 1992, along with the trends derived from our 2-D model using the same 14-year period (Figure 4b). Like the profile ozone derived trends, both these model and observed trends were derived using a linear regression model consisting of the seasonal cycle, linear trend, QBO, and 11-year solar cycle as discussed in a number of papers [e.g., *Hollandsworth et al.*, 1995]. The period after June 1991 has been influenced by the Mount Pinatubo volcano, and our 2-D model simulation contains that effect (see discussion in section 5.3). The shaded areas in the derived TOMS trends indicate regions where there is no statistically significant trend. Both the model and measurements show relatively small negative trends (0 to −2%/decade) in the tropics. The very large negative trends (over −10%/decade) poleward of 60°S in the spring are indicated in both measurements and model calculations. Large southern hemisphere trends persist in the model simulations through the summer but are not apparent in the measurements.

Between 30°N and 50°N in the winter–spring, the TOMS derived trends are about −4 to −6%/decade, whereas the computed trends are −3 to −4%/decade. The TOMS derived trend shows a peak near 45°N, whereas the model shows a peak poleward of 65°N. These TOMS derived trends in northern midlatitudes are somewhat dependent on the period analyzed and can vary by a couple of percent (S. M. Hollandsworth, private communication, 1996). The derived 2-D model trends are larger (by 1–2%) than the TOMS derived trends at northern midlatitudes in the summer and fall seasons. Combining these larger modeled trends compared to TOMS in summer–fall with the smaller modeled trends compared to TOMS in winter–spring results in an approximate cancellation in an annually averaged sense.

Much of the focus in recent years has been on the discrepancy between derived trends from model simulations and those derived from TOMS in the winter–spring at northern midlatitudes. *Chandra et al.* [1996] point out that the trends at these

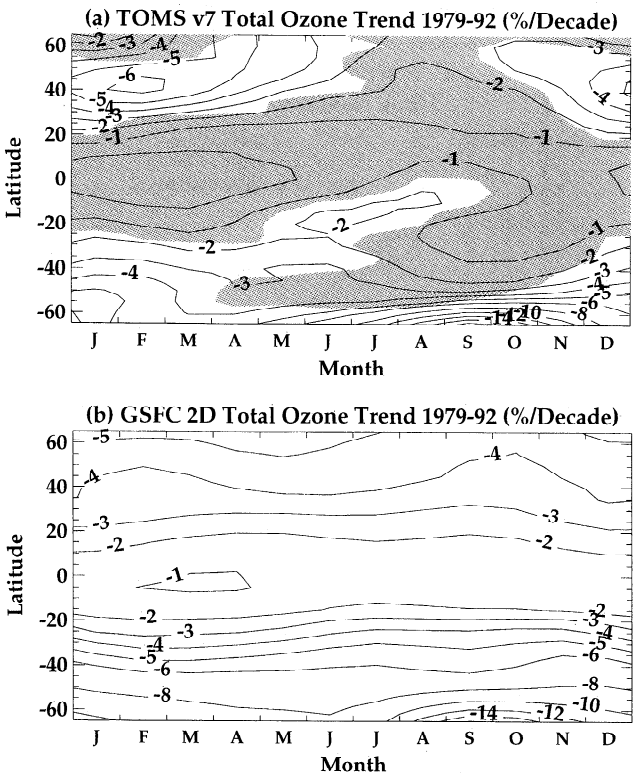

Figure 4. Total ozone derived trends for the time period 1979–1992 as a function of latitude and month of the year for (a) TOMS version 7 and (b) the GSFC 2-D model. The trends were derived using a linear regression technique described in the text. The shaded areas in the derived TOMS trends (Figure 4a) indicate regions where there is no statistically significant trend.

latitudes in the winter are also affected by the dynamically induced interannual variability, which could bias the linear trend during the TOMS observing period. *Chandra et al.* [1996] derive northern midlatitude trends of −3.7 ± −2.5%/decade from a regression model using lower stratospheric temperature as an index of dynamical variability with TOMS version 6 data. *Hood and Zaff* [1995] argue that some of the seasonal and longitudinal anomalies in TOMS derived trends could be from dynamical perturbations of tropospheric origin.

We also compare the derived 2-D model and TOMS trends at other latitudes. The derived trends from the 2-D model are slightly larger in the tropics (by 1–2%) and are somewhat larger at southern middle and high latitudes (by 2–4%) than those derived from measurements. The importance of the difference between the measurements and our model in the tropics is unclear, since the TOMS derived trend is not statistically significant in most of the tropics. The differences in the derived trends between the measurements and the 2-D model in the summer–fall southern middle and high latitudes may be related to our inability to properly simulate the spring breakup of the Antarctic polar ozone minimum.

5. Long-Term Temporal Total Ozone Variations

5.1. Anthropogenic Chlorine and Bromine Increases

Although there are some absolute differences, our model-simulated total ozone trends are qualitatively very similar to

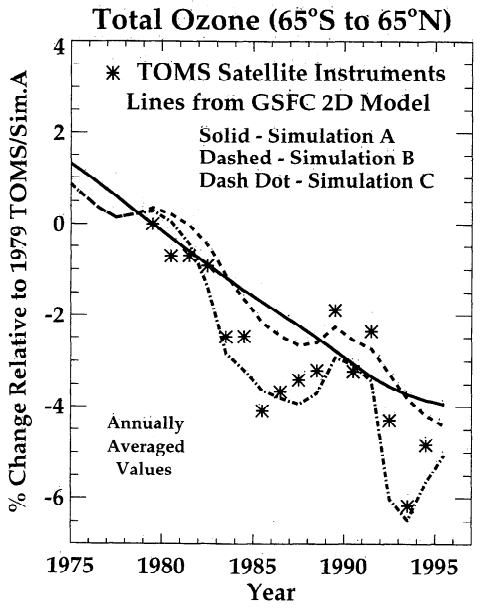

Figure 5. Percentage total ozone changes in the latitude range 65°S to 65°N for TOMS version 7 relative to the 1979 TOMS value (represented by stars). Also shown are percentage total ozone changes for simulations A (chlorine and bromine increases only; solid line), B (chlorine and bromine increases and solar UV flux variations; dashed line), and C (chlorine and bromine increases, solar UV flux variations, and SSA burden variations; dash-dot line) from the GSFC 2-D model, all relative to the 1979 simulation A value.

the version 7 TOMS derived trends. To better understand the natural and anthropogenic processes and their influence on the year-to-year variations in total ozone, we compare the annual mean TOMS total ozone averaged over 65°S and 65°N with all of these variations included, to our model simulations in Figure 5.

We first use our model in a very straightforward way and include only anthropogenic chlorine and bromine increases varied according to Table 6-3 of WMO [1995]. We designate this model calculation as simulation A (Table 1) and represent this computation by the solid line in Figure 5. The TOMS data are represented by the stars. We include both Nimbus 7 and Meteor 3 TOMS data in this comparison (McPeters et al., submitted manuscript, 1996). Both the data and model predictions are normalized to a percentage change relative to 1979. Model simulation A predicts a decrease in ozone of about 4% from year 1979 to 1995. Although there is a large amount of variability in the TOMS data from year to year, the observations show a general downward trend that is reasonably well represented by this model calculation.

Table 1. List of Model Simulations for Comparison to the Annually Averaged Global Total Ozone

Simulation	Atmospheric Perturbations
A	chlorine and bromine increases
B	ultraviolet flux variations chlorine and bromine increases
C	stratospheric sulfate aerosol surface area variation, ultraviolet flux variations, chlorine and bromine increases
D	solar proton events, stratospheric sulfate aerosol surface area variation, ultraviolet flux variations, chlorine and bromine increases
E	galactic cosmic rays, solar proton events, stratospheric sulfate aerosol surface area variation, ultraviolet flux variations, chlorine and bromine increases

In the next four subsections we address the question of whether improved agreement between the model calculation and TOMS observations is obtained by adding other atmospheric perturbations in addition to changing halocarbon fluxes. These perturbations are variations in ultraviolet solar flux, stratospheric sulfate aerosol burden, solar proton events, and galactic cosmic rays. A summary of the model simulations employed to represent the natural and anthropogenic atmospheric variations is given in Table 1.

5.2. Solar Ultraviolet Flux Variation

Solar ultraviolet flux provides the primary production of ozone in the stratosphere through photolysis of O_2 (wavelengths shorter than 242 nm) and subsequent recombination of O and O_2 in the presence of a third body. Since the solar UV flux has been observed to vary during the 11-year solar cycle and 27-day solar rotation, it has been predicted and observed that ozone in the stratosphere varies with these periods [e.g., *Garcia et al.*, 1984; *Hood et al.*, 1993; *Huang and Brasseur*, 1993; *Chandra and McPeters*, 1994; *Fleming et al.*, 1995]. Because of the difficulty in characterizing long-term changes in the solar UV spectral irradiance, the observational studies, in general, have relied on solar proxies such as ground-based solar radio flux measurements ($F10.7$ cm), available since 1947, and satellite-based MgII index data, available since 1979. The MgII index is calculated from the ratio of intensities in the center of wings of the unresolved MgII h and k solar absorption lines near 280 nm [*Heath and Schlesinger*, 1986]. These solar proxies, unfortunately, can not be used in theoretical models that require detailed characterization of the solar UV spectrum.

In a recent paper, *Chandra et al.* [1995b] have derived scale

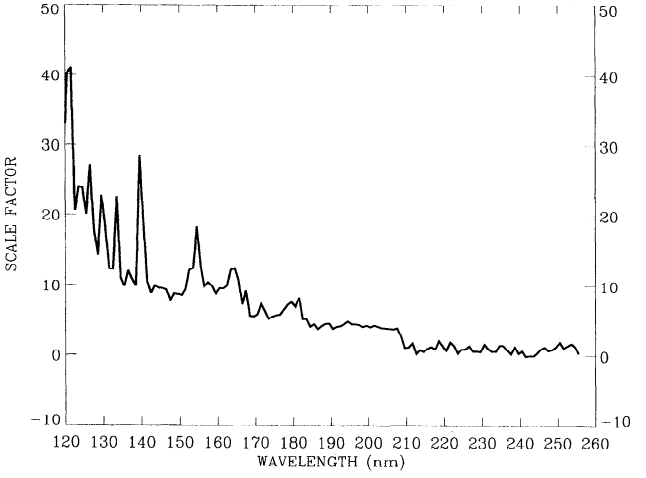

Figure 6. The 10.7-cm flux scale factor for the UV spectral irradiance derived from the UARS SOLSTICE daily spectra. The scale factor is given as a percentage change in UV irradiance for a 100-unit (1 unit = 10^{-22} W m^{-2} Hz^{-1}) change in 10.7-cm flux.

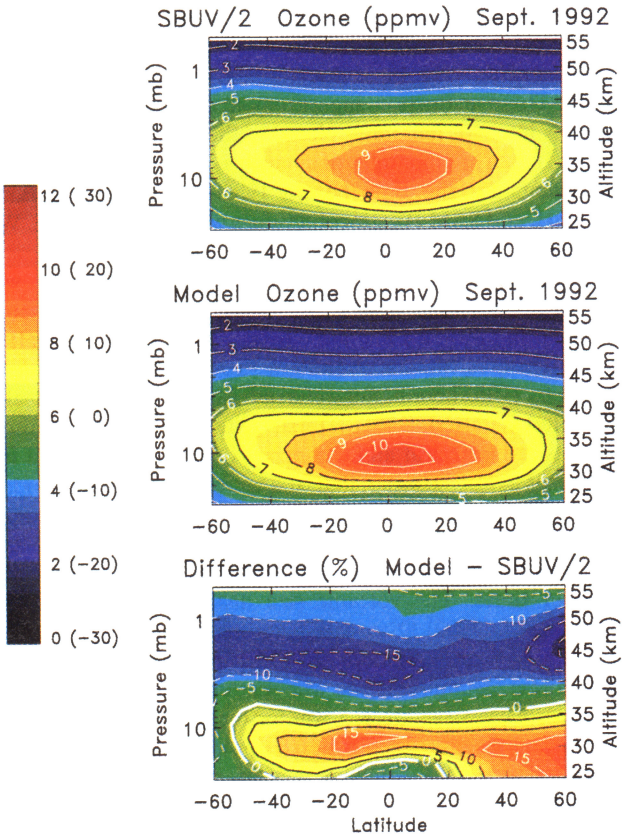

Plate 4. Zonal average ozone for September 1992 from (top) NOAA 11 SBUV/2 measurements, (middle) the GSFC 2-D model, and (bottom) the percentage difference between model and measurements. The scale on the color bar is in parts per million by volume (ppmv), and the percentage difference is in parentheses.

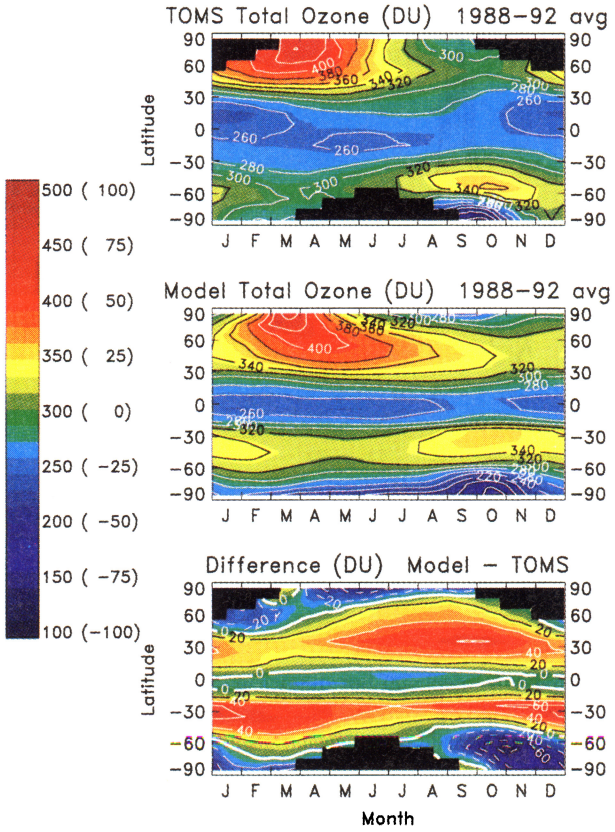

Plate 5. Total ozone as a function of latitude and month of the year taken from (top) TOMS version 7 1988–1992 average, (middle) the GSFC 2-D model, and (bottom) the difference between the model and TOMS measurements. The scale on the color bar is in Dobson units (DU), and the difference in DU is in parentheses.

factors for the spectral range 120–200 nm that can be used with the MgII index to estimate the solar irradiance change over a solar cycle. The scale factors were derived from the UV flux measured from the Solar Stellar Irradiance Comparison Experiment (SOLSTICE) and Solar Spectra Irradiance Monitor (SUSIM) instruments on the UARS. These two UARS instruments have made continuous measurements of the UV flux in the spectral range 115–420 nm since October 1991 and cover the declining phase of solar cycle 22 from near-maximum to near-minimum solar activity levels. Since the data on MgII index are not available for the period before 1979, we have used the UV flux measured from the UARS and $F10.7$ to derive scale factors following *Chandra et al.* [1995b]. This analysis makes it possible to derive the UV flux changes using 10.7-cm flux variations as a transfer standard for non-UARS observing years beginning from 1947.

Figure 6 shows the $F10.7$ scale factors derived from the SOLSTICE daily spectra from October 1991 to December 1994. The scale factors are given as a percentage change in UV flux in the range 120–255 nm (with 1-nm resolution) for a change in 100 units of $F10.7$. The peaks in the scale factors correspond to the emission lines in this spectral range. Average scale factors (expressed as percentage change per 100 unit change in $F10.7$) are 40.6 for the Lyman α band centered on 121.6 nm, 14.6 for the band 125–150 nm, 9.4 for the band 150–175 nm, 5.1 for the band 175–200 nm, 4.1 for the band 200–205 nm, and 1.2 for the band 205–255 nm. A time history (1947 to present) of the solar cycle variation at 200 nm using $F10.7$ as a transfer standard is shown in Figure 7. This figure suggests that the solar cycles 21 and 22 (periods 1975–1985 and 1985–1995) are basically similar with respect to the changes in

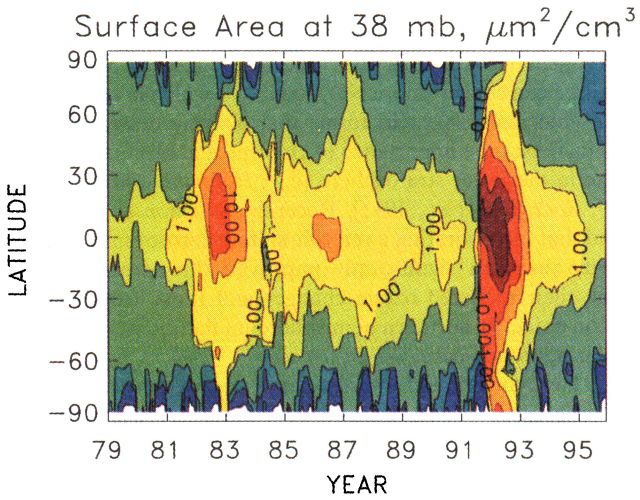

Plate 6. Surface area density interpolated to the 38-mbar model surface with the method described in the text. The contour intervals are: 0.01, 0.05, 0.1, 0.5, 1.0, 5.0, 10.0, 20.0, and 30.0 $\mu m^2\ cm^{-3}$. The year tick marks correspond to the first day of the year.

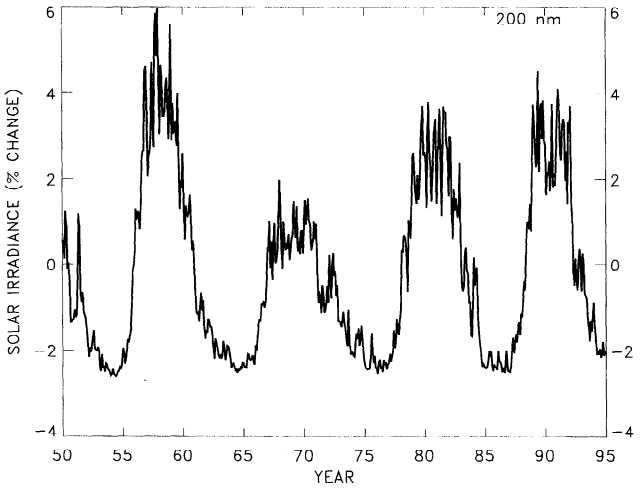

Figure 7. Percentage change in solar irradiance at 200 nm with respect to the mean of the entire measurement record (1947–1995), calculated from the monthly values of 10.7-cm flux and the 10.7-cm flux scale factor as discussed in the text.

the solar UV spectrum but differ significantly with respect to the preceding two solar cycles.

Our model prediction including the solar UV flux variation along with chlorine and bromine increases for the 1975 to 1995 period is designated simulation B and is represented by the dashed line in Figure 5. The effect of the solar UV flux variation on total ozone in the 65°S to 65°N region is found to be a maximum of ±0.6% (about 1.2% from solar maximum to minimum) and is calculated when the total ozone computed in simulation B is subtracted from that of simulation A. Qualitatively and quantitatively it appears that more of the year-to-year change in the TOMS data is better represented in this model simulation which includes the solar cycle UV variation.

5.3. Stratospheric Sulfate Aerosol Effects

The stratospheric sulfate aerosol burden has changed significantly between 1979 and 1995. Two major volcanic eruptions (El Chichón in April 1982 and Mount Pinatubo in June 1991), as well as several minor eruptions, occurred, sometimes resulting in dramatic increases in the SSA burden [e.g., *Hofmann*, 1987; *McCormick*, 1992; *Bluth et al.*, 1992; *Trepte et al.*, 1993]. Heterogeneous reactions promoted by the increased SSA surface area can convert more NO_x to HNO_3, which in turn allows more chlorine to exist in forms that actively destroy ozone. This increases the importance of chlorine and bromine loss for ozone in the lower stratosphere [e.g., *Hofmann and Solomon*, 1989; *Rodriguez et al.*, 1991]. Recently, *Solomon et al.* [1996] found that incorporating a realistic sulfate aerosol surface area density variation significantly improved the agreement between their modeled ozone changes and those from TOMS version 6 data at northern hemisphere midlatitudes. We take a similar approach here.

We have constructed a surface area density time history for the time period 1979–1995 using extinction measurements from SAGE I, SAGE II, SAM II, and SME data. The SAM II data consist of monthly zonal mean 1-μm aerosol extinction measurements at high latitudes in both the southern and northern hemispheres and extend from 1979 through 1995. The SAGE I data are monthly zonal mean measurements of 1-μm aerosol extinction coefficients made between 1979 and 1981. The SME data consist of weekly zonal mean 6.8-μm aerosol extinction coefficients for the time period 1982–1984 [*Eparvier et al.*, 1994; F. G. Eparvier, personal communication, 1996]. These extinction measurements were averaged into monthly intervals and interpolated to the SAGE I/II grid. The SAGE II data are monthly zonal mean 1-μm aerosol extinction coefficients for the time period 1985–1995. The SAGE I, SAGE II, and SAM II extinction values were provided by L. W. Thomason (NASA Langley Research Center).

To convert the extinction data to surface area density, we use the methodology of J. E. Rosenfield et al. (Stratospheric effects of the Mount Pinatubo aerosol studied with a coupled two-dimensional model, submitted to *Journal of Geophysical Research*, 1996, hereinafter referred to as Rosenfield et al., submitted manuscript, 1996). First, we assume that the aerosol droplets are spherical and composed of 75% sulfuric acid by weight. We also assume that the aerosols obey a bimodal lognormal distribution during periods of high aerosol loading (April 1982 through December 1984 and June 1991 through December 1995) and a unimodal background size distribution at other times. The volcanic size distribution was from a *Deshler et al.* [1993] fit to data taken on August 2, 1991. The background size distribution is taken from *Hofmann* [1990]. Using these assumptions and Mie scattering theory, we derive the aerosol cross section at 1 μm for the SAGE I/II and SAM II data, and the cross section at 6.8 μm for the SME data. This cross section and the extinction measurements are then used to obtain an aerosol number density that varies in time and space. From the estimated aerosol number density and the assumed distributions, an estimate of the surface area density is obtained.

The estimates of background surface area density obtained from the SME extinction data using the above method are significantly higher than those obtained from the SAM II and SAGE I/II data. We therefore chose to scale the surface area density values calculated from the SME data to the surface area density from the SAGE data. At each altitude we determined the ratio of the average SAGE surface area density in January 1985 to the average SME surface area density in January 1984. All the SME data were then adjusted using these ratios.

The SME data extend from 20 to 36 km in altitude. In order to obtain a surface area density estimate between 20 km and the tropopause during the period between the eruption of El Chichón and the end of 1984, we used surface area density estimates from after the Mount Pinatubo eruption divided by 3. The factor of 3 corresponds roughly to the difference in stratospheric mass loading caused by the two volcanic eruptions [*WMO*, 1995].

Since there were many months where the SAGE observations did not cover a full latitude range, we took a 3-month running median through the monthly data before interpolating the data set to the model's latitude and pressure grid. A plot of the surface area density obtained for the 38-mbar model level is shown in Plate 6. The surface area density estimates compare reasonably well with the more sophisticated multiple wavelength surface area density calculations of *Thomason et al.* [1996] during the SAGE II time period. The two calculations generally agree during the entire 10-year period to within 20 or 30% up to about 25 km in the tropics and up to about 22 km at middle and higher latitudes. Our calculation is typically somewhat lower than that of *Thomason et al.* [1996]. The agreement worsens in regions and times of low aerosol loading

such as at high altitudes, with typical discrepancies of a factor of 2. This may be due to our neglect of spatial and temporal variation in the aerosol size distributions used to convert extinction to surface area density.

The major difference between our calculated surface area densities and those used in the *Solomon et al.* [1996] study occur between 1982 and 1984. During this time, *Solomon et al.* [1996] used one of two constant values bracketing the possible range of El Chichón values, while we estimate the surface area density using SME aerosol extinction measurements as described above.

The derived surface areas of SSA for the time period 1979–1995 were input into our 2-D model, which also included the solar UV flux variation and the chlorine and bromine increases. This model prediction is designated simulation C and is represented by the dashed-dotted line in Figure 5. The maximum effect of the SSA burden on total ozone in the 65°S to 65°N region is an additional decrease of about 2.8% in 1992 over model run B, which includes halocarbon and solar ultraviolet variations. Total ozone remains low in the model in 1993 as a result of the increased aerosols, producing reasonable agreement with the TOMS total ozone for this year. The addition of the derived SSA over the TOMS observing period into our model results in a much better model-measurement comparison.

The effects of the sulfate aerosol on heating and photolysis rates have not been taken into account in this study. These perturbations, as well as the heterogeneous chemistry perturbation, have been included in a study of the effects of the Mount Pinatubo volcanic aerosol using our new interactive chemical-radiative-dynamical two-dimensional model (Rosenfield et al., submitted manuscript, 1996). The maximum globally averaged column ozone depletion with the full perturbation was found to be 3.7%, with the heating rate and photolysis rate perturbations each contributing less than 0.5%. However, the changes due to heating rate and photolysis effects for average aerosol loading during 1979–1995 should be significantly less than 0.5%, so that such effects will not significantly change the results of this study.

5.4. Solar Proton Event Effects

The influence of large solar proton events on ozone over long time periods has been addressed before [e.g., *Jackman et al.*, 1990; *Reid et al.*, 1991]. SPEs can dissociate N_2, which leads to increases in long-lived odd nitrogen constituents. SPEs also produce ions which cause enhancements of short-lived HO_x (H, OH, HO_2) constituents after complicated ion chemistry. Both odd nitrogen and HO_x constituents lead to associated decreases in ozone. Although upper stratospheric ozone in the polar cap is predicted and measured to be reduced by over 20% as a result of extremely large SPEs, total ozone is predicted to be decreased by a maximum of 4% only poleward of 75°N [*Jackman et al.*, 1995a].

We use *Vitt and Jackman* [1996] ionization rates and assume that 1.25 nitrogen atoms are produced per ion pair [*Porter et al.*, 1976; *Jackman et al.*, 1980] to compute the odd nitrogen produced by SPEs from 1975 to 1993. The SPE-produced HO_x was included in our 2-D model simulation in the following ways: (1) below 70 km, each ion pair was assumed to result in the formation of two HO_x species, and (2) above 70 km the HO_x species production per ion pair was taken from *Solomon et al.* [1981, Figure 2].

We have computed the odd nitrogen and HO_x produced by the SPEs and have input these sources into our model calculation, which also includes the derived surface areas of SSA, the solar UV flux variation, and the chlorine and bromine increases. This model calculation is designated as simulation D. The effect of the SPEs on total ozone in the 65°S to 65°N region can be observed most easily when the total ozone computed in simulation D is subtracted from that of simulation C and plotted as the dashed line in Figure 8b. The yearly mean sunspot number is plotted in Figure 8a to show the correlation between SPEs and solar cycle. In general, most large SPEs that lead to total ozone change occur near solar maximum.

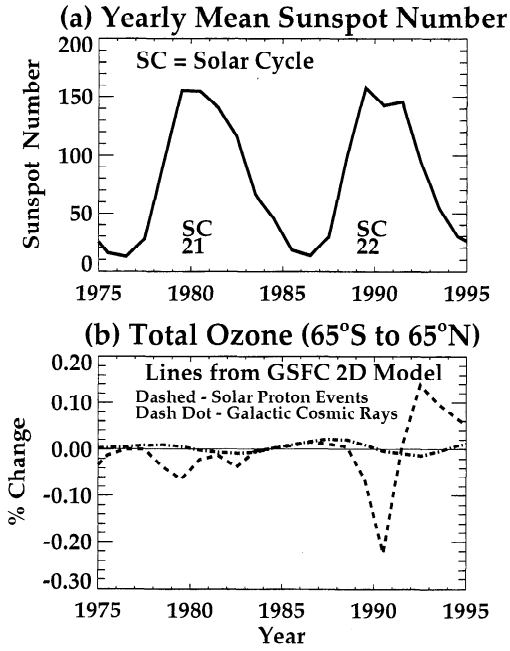

Figure 8. (a) Yearly mean international sunspot number taken from the Solar Geophysical Data publication. (b) GSFC 2-D model-predicted total ozone variation as a result of solar proton events (dashed line) and galactic cosmic rays (dash-dot line).

The long-term and middle-lower stratospheric ozone changes are caused by the NO_x produced by the SPEs. The largest total ozone decrease is predicted to be about 0.22% in 1990 (see Figure 8b). This particularly large ozone loss is primarily caused by the extremely large SPEs of October 1989, which created much NO_x in the upper stratosphere. Most of this ozone decrease caused by SPEs is constrained to latitudes poleward of 50°.

As the upper stratospheric SPE-produced NO_x is transported over the next several months to lower altitudes, the interference with the chlorine and bromine loss cycles for ozone destruction become important. This is especially true when background stratospheric chlorine levels rise higher than about 2.5 ppbv (years since 1985) and SPE-induced ozone changes are predicted to be positive during certain years (e.g., 1992–1994).

5.5. Galactic Cosmic Ray Effects

Galactic cosmic rays also produce odd nitrogen and HO_x. The GCRs primarily affect the lower stratosphere and upper troposphere; they form odd nitrogen via dissociation of N_2 and form HO_x via complicated ion chemistry on GCR-produced ions. We use the methodology of *Vitt and Jackman* [1996] to

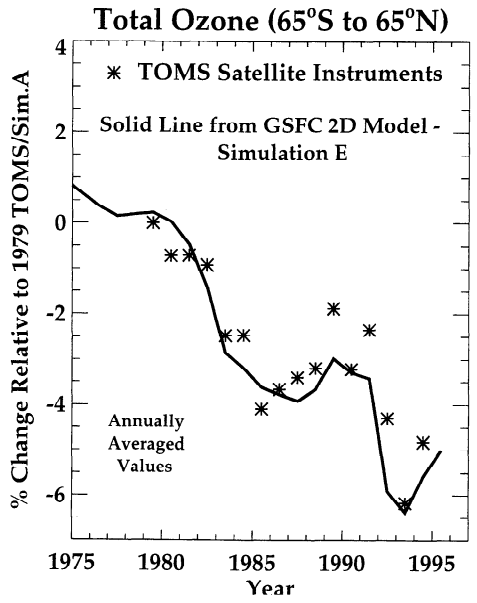

Figure 9. Percentage total ozone changes in the 65°S to 65°N latitude range for TOMS version 7 relative to the 1979 TOMS value (represented by stars). Also shown are percentage total ozone changes for simulation E (chlorine and bromine increases, solar UV flux variations, SSA burden variations, solar proton events, and galactic cosmic rays) from the GSFC 2-D model, all relative to the 1979 simulation A value.

derive the ion pair production resulting from GCR fluxes during the time period 1957–1995, scaling by sunspot number measurements. The GCR flux is anticorrelated with the sunspot number; thus the maximum GCR flux occurs near sunspot minimum. Odd nitrogen from GCRs, as from SPEs, is assumed to be produced at the rate of 1.25 nitrogen atoms per ion pair. We assume that two HO_x constituents are produced per ion pair. The GCR-produced odd nitrogen and HO_x, SPE-produced odd nitrogen and HO_x, the derived surface areas of SSA, the solar UV flux variation, and the chlorine and bromine increases are all included in our 2-D model simulation designated as simulation E. This simulation E is the same as our standard simulation.

The effect of the GCRs on total ozone in the 65°S to 65°N region can be observed most easily when the total ozone computed in simulation E is subtracted from that of simulation D and plotted as the dashed-dotted line in Figure 8b. The largest total ozone decrease or increase is predicted to be about +0.02% and occurs in 1987 (see Figure 8b). Like the SPEs, and as is discussed by *Jackman et al.* [1995b], the increased GCR production of odd nitrogen and HO_x near solar minimum generally leads to an increase of ozone in years when stratospheric chlorine levels are more than about 2.5 ppbv (years since 1985) because of interference with the ozone loss caused by chlorine and bromine constituents. However, as can be seen in Figure 8b, the effect of the temporal change in the GCR flux on total ozone is quite small.

6. Discussion and Conclusions

Simulation E (the "standard" simulation) is our most complete simulation of the effects of anthropogenic and natural influences on total ozone and includes chlorine and bromine increases, the solar UV flux variation, the derived surface areas of SSA, SPE-produced odd nitrogen and HO_x, and GCR-produced odd nitrogen and HO_x. We show this model prediction in Figure 9, where it is represented by the solid line. With the inclusion of sources of ozone variability other than halocarbon increases, much of the year-to-year behavior in TOMS observations is captured by this simulation. The total ozone changes in some years (e.g., 1989 and 1991) are obviously not well simulated. Our model has seasonally varying transport fields, which repeat for each year of the simulation. It is possible that interannual dynamical variability including the QBO, as well as a dynamical response to halocarbon-induced changes in ozone, could be responsible for some of the differences between the model and measurements seen in Figure 9.

Natural processes like GCRs, SPEs, solar UV flux variations and volcanoes do have some influence on ozone levels. GCRs are computed to cause relatively minuscule variations of a maximum of +0.02% in annually averaged almost global total ozone (AAGTO) over a solar cycle. The AAGTO is computed by annually averaging the total ozone between 65°S and 65°N. SPEs are predicted to cause somewhat more AAGTO change (maximum of 0.22% decrease) during extremely large events. Solar UV flux variations are calculated to provide a moderate perturbation to the AAGTO over a solar cycle with a maximum of ±0.6% (about 1.2% from solar maximum to minimum). Major volcanic eruptions can have significant effects on ozone and were computed to result in a maximum decrease of about 2.8% in the AAGTO.

The largest anthropogenic effect on ozone is that due to halocarbon emissions. Our simulations predict that AAGTO decreases about 4% from year 1979 to 1995 as a result of these chlorine and bromine emissions. We continued the simulation A computations for 35 more years up to year 2030 using Table 6-3 of *WMO* [1995] for surface boundary conditions of halocarbons and other important source gases. The results of this simulation are shown in Figure 10. The ground source gas boundary conditions for chlorine and bromine peak in years 1994 and 1995, respectively [see *WMO*, 1995]. It has recently been shown that the tropospheric chlorine levels peaked in early 1994 [*Montzka et al.*, 1996], very close to the levels assumed by *WMO* [1995] and in this study. The model predictions are represented by the solid line, and the TOMS measurements are indicated by the stars. The dashed lines indicate a ±1% variation around the future ozone predictions to roughly approximate the interannual ozone variations that might be expected, given the past variations in the TOMS total ozone measurements.

Ozone is predicted to reach its minimum levels in 1996 and slowly recover after that, achieving 1980 levels sometime between 2010 and 2030, depending on natural variability. The recovery of ozone is affected not only by decreases in the stratospheric loading of chlorine and bromine, but also by the CH_4 and N_2O increases, which are also driven by their surface boundary condition growth. Both CH_4 and N_2O help to mitigate halogen influence on ozone by tying up the halogens in reservoir form via the following mechanisms:

1. The more important mechanism is the reaction of CH_4 with Cl to form HCl, a reservoir of chlorine. CH_4 is assumed to be increasing more than N_2O in the future [see *WMO*, 1995, Table 6-3].

2. N_2O can react with $O(^1D)$ to form NO. NO can very quickly form NO_2 through reaction with O_3. The NO_2 then can form reservoirs $ClONO_2$ or $BrONO_2$ through reaction with a third body and ClO or BrO, respectively. Thus increases in

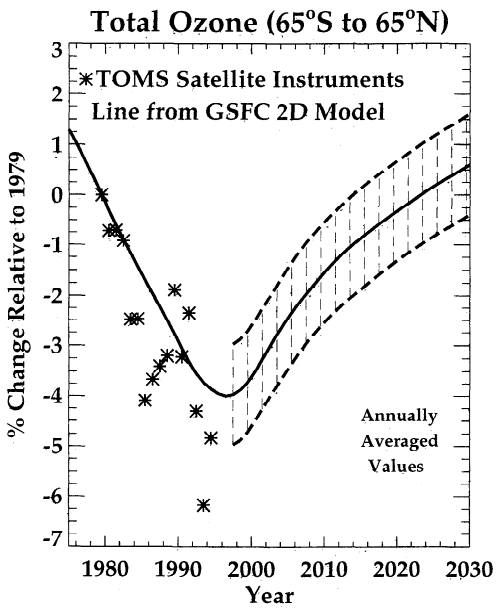

Figure 10. Percentage total ozone changes in the 65°S to 65°N latitude range for TOMS version 7 relative to the 1979 TOMS value (represented by stars). Also shown are percentage total ozone changes for simulation A (chlorine and bromine increases only) for the years 1975–2030, all relative to the 1979 simulation A value. Simulation A is represented by the solid line; for the years 1997–2030 the dashed lines represent simulation A ±1%.

N_2O reduce the effects of increases in chlorine and bromine loading. It should be noted that increases in N_2O also produce small increases in ozone destruction by odd nitrogen chemistry. This effect is relatively small over the time period being simulated.

The model predictions in Figure 10 represent our best attempt to simulate the effects of halocarbon releases on ozone in the past, present, and future. It is obviously true that these future predictions of ozone change depend on the assumed source gas trends. It is not possible to know whether future source gas boundary conditions will follow those that have been assumed. Although our 2-D model does a reasonable job of predicting the past trends in total ozone, there are known difficulties with present-day atmospheric model predictions. Problems in predicting upper stratospheric ClO, ozone, profile ozone trends, and middle northern latitude total ozone trends have been discussed. Future work should focus on resolving these modeling difficulties.

Acknowledgments. We would like to acknowledge several people for helpful contributions to this paper. Lance E. Deaver (NASA Langley Research Center) and James M. Russell III (Hampton University) provided UARS HALOE data, and Michael R. Gunson (Jet Propulsion Laboratory) sent ATMOS data for HCl and HF. Richard S. Stolarski (NASA Goddard Space Flight Center) provided TOMS version 7 annually averaged total ozone values, and Stacey M. Hollandsworth (Applied Research Corporation) supplied some early TOMS version 7 total ozone derived trends used in this study. Jerry R. Ziemke (NASA Goddard Space Flight Center) derived profile and total ozone trends from the SBUV, SBUV/2, and TOMS measurements and our 2-D model simulations using the same regression analysis technique. Larry W. Thomason (NASA Langley Research Center) provided the SAGE I/II and SAM II extinction data, and Francis G. Eparvier (NOAA Space Environment Center) provided the SME extinction coefficients used to construct the SSA surface area density distribution. The SBUV, SBUV/2, TOMS, ATMOS, SAGE I and II, SAM II, SME, Sonde, Umkehr, UARS HALOE, UARS MLS, and UARS CLAES teams are all gratefully acknowledged for their hard work in providing extremely useful atmospheric measurements. We thank NASA Headquarters Atmospheric Chemistry Modeling and Analysis Program for support during the time that this project was undertaken. We acknowledge two anonymous reviewers for helpful suggestions.

References

Anderson, D. E., Jr., and S. A. Lloyd, Polar twilight UV-visible radiation field: Perturbations due to multiple scattering, ozone depletion, stratospheric clouds, and surface albedo, *J. Geophys. Res.*, *95*, 7429–7434, 1990.

Anderson, D. E., Jr., and R. R. Meier, Effects of anisotropic multiple scattering on solar radiation in the troposphere and stratosphere, *Appl. Opt.*, *18*, 1955–1960, 1979.

Andrews, D. G., J. R. Holton, and C. B. Leovy, *Middle Atmosphere Dynamics*, 498 pp., Academic, San Diego, Calif., 1987.

Bacmeister, J. T., M. R. Schoeberl, M. E. Summers, J. E. Rosenfield, and X. Zhu, Descent of long-lived trace gases in the winter polar vortex, *J. Geophys. Res.*, *100*, 11,669–11,684, 1995.

Barnett, J. J., and K. Labitzke, Climatological distribution of planetary waves in the middle atmosphere, *Adv. Space Res.*, *10*(12), 63–91, 1990.

Bluth, G. J. S., S. D. Doiron, A. J. Krueger, L. S. Walter, and C. C. Schnetzler, Global tracking of the SO_2 cloud from the June 1991 Mt. Pinatubo eruptions, *Geophys. Res. Lett.*, *19*, 151–154, 1992.

Bojkov, R. D., L. Bishop, W. J. Hill, G. C. Reinsel, and G. C. Tiao, A statistical trend analysis of revised Dobson total ozone data over the northern hemisphere, *J. Geophys. Res.*, *95*, 9785–9807, 1990.

Brasseur, G., and C. Granier, Mount Pinatubo acrosols, chlorofluorocarbons, and ozone depletion, *Science*, *257*, 1239–1242, 1992.

Callis, L. B., R. E. Boughner, M. Natarajan, J. D. Lambeth, D. N. Baker, and J. B. Blake, Ozone depletion in the high latitude lower stratosphere: 1979–1990, *J. Geophys. Res.*, *96*, 2921–2937, 1991.

Carpenter, R. L., Jr., K. K. Droegemeier, P. R. Woodward, and C. E. Hane, Application of the piecewise parabolic method (PPM) to meteorological modeling, *Mon. Weather Rev.*, *118*, 586–612, 1990.

Chandra, S., and R. D. McPeters, The solar cycle variation of ozone in the stratosphere inferred from Nimbus 7 and NOAA 11 satellites, *J. Geophys. Res.*, *99*, 20,665–20,671, 1994.

Chandra, S., C. H. Jackman, A. R. Douglass, E. L. Fleming, and D. B. Considine, Chlorine-catalyzed destruction of ozone: Implications for ozone variability in the upper stratosphere, *Geophys. Res. Lett.*, *20*, 351–354, 1993.

Chandra, S., C. H. Jackman, and E. L. Fleming, Recent trends in ozone in the upper stratosphere: Implications for chlorine chemistry, *Geophys. Res. Lett.*, *22*, 843–846, 1995a.

Chandra, S., J. L. Lean, O. R. White, D. K. Prinz, G. J. Rottman, and G. E. Brueckner, Solar UV irradiance variability during the declining phase of the solar cycle 22, *Geophys. Res. Lett.*, *22*, 2481–2484, 1995b.

Chandra, S., C. Varotsos, and L. E. Flynn, The mid-latitude total ozone trends in the northern hemisphere, *Geophys. Res. Lett.*, *23*, 555–558, 1996.

Colella, P., and P. R. Woodward, The piecewise parabolic method (PPM) for gasdynamical simulations, *J. Comput. Phys.*, *54*, 174–201, 1984.

Considine, D. B., A. R. Douglass, and C. H. Jackman, Effects of a polar stratospheric cloud parameterization on ozone depletion due to stratospheric aircraft in a two-dimensional model, *J. Geophys. Res.*, *99*, 18,879–18,894, 1994.

Cunnold, D. M., P. J. Fraser, R. F. Weiss, R. G. Prinn, P. G. Simmonds, B. R. Miller, F. N. Alyea, and A. J. Crawford, Global trends and annual releases of CCl_3F and CCl_2F_2 estimated from ALE/GAGE and other measurements from July 1978 to June 1991, *J. Geophys. Res.*, *99*, 1107–1126, 1994.

Delisi, D. P., and T. J. Dunkerton, Seasonal variation of the semiannual oscillation, *J. Atmos. Sci.*, *45*, 2772–2787, 1988.

DeMore, W. B., D. M. Golden, R. F. Hampson, C. J. Howard, C. E. Kolb, M. J. Kurylo, M. J. Molina, A. R. Ravishankara, and S. P. Sander, Chemical kinetics and photochemical data for use in stratospheric modeling, Evaluation number 11, *JPL Publ.*, *94-26*, 273 pp., 1994.

De Rudder, A., N. Larsen, X. Tie, G. P. Brasseur, and C. Granier,

Model study of polar stratospheric clouds and their effect on stratospheric ozone, 1, Model description, *J. Geophys. Res.*, *101*, 12,567–12,574, 1996.

Deshler, T., B. J. Johnson, and W. R. Rozier, Balloonborne measurements of Pinatubo aerosol during 1991 and 1992 at 41°N: Vertical profiles, size distribution, and volatility, *Geophys. Res. Lett.*, *20*, 1435–1438, 1993.

Dessler, A. E., S. R. Kawa, D. B. Considine, J. W. Waters, L. Froidevaux, and J. B. Kumer, UARS measurements of ClO and NO_2 at 40 and 46 km and implications for the model "ozone deficit," *Geophys. Res. Lett.*, *23*, 339–342, 1996.

Douglass, A. R., C. H. Jackman, and R. S. Stolarski, Comparison of model results transporting the odd nitrogen family with results transporting separate odd nitrogen species, *J. Geophys. Res.*, *94*, 9862–9872, 1989.

Dunkerton, T. J., On the role of the Kelvin wave in the westerly phase of the semiannual zonal wind oscillation, *J. Atmos. Sci.*, *36*, 32–41, 1979.

Elkins, J. W., T. M. Thompson, T. H. Swanson, J. H. Butler, D. B. Hall, S. O. Cummings, D. A. Fisher, and A. G. Raffo, Decrease in the growth rates of atmospheric chlorofluorocarbons-11 and -12, *Nature*, *364*, 780–783, 1993.

Eluszkiewicz, J., and M. Allen, A global analysis of the ozone deficit in the upper stratosphere and lower mesosphere, *J. Geophys. Res.*, *98*, 1069–1082, 1993.

Eparvier, F. G., D. W. Rusch, R. T. Clancy, and G. E. Thomas, Solar Mesosphere Explorer satellite measurements of El Chichón stratospheric aerosols, 2, Aerosol mass and size parameters, *J. Geophys. Res.*, *99*, 20,533–20,544, 1994.

Fleming, E. L., S. Chandra, J. J. Barnett, and M. Corney, Zonal mean temperature, pressure, zonal wind, and geopotential height as functions of latitude, *Adv. Space Res.*, *10*(12), 11–59, 1990.

Fleming, E. L., S. Chandra, C. H. Jackman, D. B. Considine, and A. R. Douglass, The middle atmospheric response to short and long term solar UV variations: Analysis of observations and 2D model results, *J. Atmos. Terr. Phys.*, *57*, 333–365, 1995.

Garcia, R. R., and S. Solomon, A numerical model of the zonally averaged dynamical and chemical structure of the middle atmosphere, *J. Geophys. Res.*, *88*, 1379–1400, 1983.

Garcia, R. R., S. Solomon, R. G. Roble, and D. W. Rusch, A numerical response of the middle atmosphere to the 11-year solar cycle, *Planet. Space Sci.*, *32*, 411–423, 1984.

Garcia, R. R., F. Stordal, S. Solomon, and J. T. Kiehl, A new numerical model of the middle atmosphere, 1, Dynamics and transport of tropospheric source gases, *J. Geophys. Res.*, *97*, 12,967–12,991, 1992.

Gleason, J. F., et al., Record low global ozone in 1992, *Science*, *260*, 523–526, 1993.

Gray, L. J., and T. J. Dunkerton, The role of the seasonal cycle in the quasi-biennial oscillation of ozone, *J. Atmos. Sci.*, *47*, 2429–2451, 1990.

Gray, L. J., and J. A. Pyle, Two-dimensional model studies of equatorial dynamics and tracer distributions, *Q. J. R. Meteorol. Soc.*, *113*, 635–651, 1987.

Gray, L. J., and J. A. Pyle, A two-dimensional mean circulation model of the quasi-biennial oscillation of ozone, *J. Atmos. Sci.*, *46*, 203–220, 1989.

Gunson, M. R., M. C. Abrams, L. L. L. Lowes, E. Mahieu, R. Zander, C. P. Rinsland, M. K. W. Ko, N.-D. Sze, and D. K. Weisenstein, Increase in levels of stratospheric chlorine and fluorine loading between 1985 and 1992, *Geophys. Res. Lett.*, *21*, 2223–2226, 1994.

Hanson, D. R., and A. R. Ravishankara, Reaction of $ClONO_2$ with HCl on NAT, NAD, and frozen sulfuric acid and hydrolysis of N_2O_5 and $ClONO_2$ on frozen sulfuric acid, *J. Geophys. Res.*, *98*, 22,931–22,936, 1993.

Hanson, D. R., and A. R. Ravishankara, Reactive uptake of $ClONO_2$ onto sulfuric acid due to reaction with HCl and H_2O, *J. Phys. Chem.*, *98*, 5728–5735, 1994.

Heath, D. F., and B. M. Schlesinger, The Mg-280 nm doublet as a monitor of changes in solar ultraviolet irradiance, *J. Geophys. Res.*, *91*, 8672–8682, 1986.

Hofmann, D. J., Perturbations to the global atmosphere associated with the El Chichón volcanic eruption of 1982, *Rev. Geophys.*, *25*, 743–759, 1987.

Hofmann, D. J., Increase in the stratospheric background sulfuric acid aerosol mass in the past 10 years, *Science*, *248*, 996–1000, 1990.

Hofmann, D. J., and S. Solomon, Ozone destruction through heterogeneous chemistry following the eruption of El Chichón, *J. Geophys. Res.*, *94*, 5029–5041, 1989.

Hofmann, D. J., S. J. Oltmans, W. D. Komhyr, J. M. Harris, J. A. Lathrop, A. O. Langford, T. Deshler, B. J. Johnson, A. Torres, and W. A. Matthews, Ozone loss in the lower stratosphere over the United States in 1992–1993: Evidence for heterogeneous chemistry on the Pinatubo aerosol, *Geophys. Res. Lett.*, *21*, 65–68, 1994.

Hollandsworth, S. M., R. D. McPeters, L. E. Flynn, W. Planet, A. J. Miller, and S. Chandra, Ozone trends derived from the combined Nimbus 7 SBUV and NOAA 11 SBUV/2 data, *Geophys. Res. Lett.*, *22*, 905–908, 1995.

Holton, J. R., and X. Zhu, A further study of gravity wave induced drag and diffusion in the mesosphere, *J. Atmos. Sci.*, *41*, 2653–2662, 1984.

Hood, L. L., and D. A. Zaff, Lower stratospheric stationary waves and the longitude dependence of ozone trends in winter, *J. Geophys. Res.*, *100*, 25,791–25,800, 1995.

Hood, L. L., J. L. Jirikowic, and J. P. McCormac, Quasi-decadal variability of the stratosphere: Influence of long term solar ultraviolet variations, *J. Atmos. Sci.*, *50*, 3941–3958, 1993.

Huang, T. Y. W., and G. P. Brasseur, Effect of long-term solar variability in a two-dimensional interactive model of the middle atmosphere, *J. Geophys. Res.*, *98*, 20,413–20,427, 1993.

Jackman, C. H., Energetic particle influences on NO_y and ozone in the middle atmosphere, in *Interactions Between Global Climate Subsystems, Geophys. Monogr. Ser.*, vol. 75, edited by G. A. McBean and M. Hanlel, pp. 131–139, AGU, Washington, D. C., 1993.

Jackman, C. H., and R. D. McPeters, The response of ozone to solar proton events during solar cycle 21: A theoretical interpretation, *J. Geophys. Res.*, *90*, 7955–7966, 1985.

Jackman, C. H., J. E. Frederick, and R. S. Stolarski, Production of odd nitrogen in the stratosphere and mesosphere: An intercomparison of source strengths, *J. Geophys. Res.*, *85*, 7495–7505, 1980.

Jackman, C. H., A. R. Douglass, R. B. Rood, R. D. McPeters, and P. E. Meade, Effect of solar proton events on the middle atmosphere during the past two solar cycles as computed using a two-dimensional model, *J. Geophys. Res.*, *95*, 7417–7428, 1990.

Jackman, C. H., A. R. Douglass, S. Chandra, R. S. Stolarski, J. E. Rosenfield, and J. A. Kaye, Impact of interannual variability (1979–1986) of transport and temperature on ozone as computed using a two-dimensional photochemical model, *J. Geophys. Res.*, *96*, 5073–5079, 1991a.

Jackman, C. H., A. R. Douglass, K. F. Brueske, and S. A. Klein, The influence of dynamics on two-dimensional model results: Simulations of ^{14}C and stratospheric aircraft NO_x injections, *J. Geophys. Res.*, *96*, 22,559–22,572, 1991b.

Jackman, C. H., M. C. Cerniglia, J. E. Nielsen, D. J. Allen, J. M. Zawodny, R. D. McPeters, A. R. Douglass, J. E. Rosenfield, and R. B. Rood, Two-dimensional and three-dimensional model simulations, measurements, and interpretation of the influence of the October 1989 solar proton events on the middle atmosphere, *J. Geophys. Res.*, *100*, 11,641–11,660, 1995a.

Jackman, C. H., F. M. Vitt, D. B. Considine, and E. L. Fleming, Energetic particle precipitation effects on odd nitrogen and ozone over the solar cycle time scale, in *The Solar Cycle Variation of the Stratosphere, A STEP Working Group 5 Report*, edited by L. L. Hood, Dep. of Planet. Sci., Univ. of Ariz., Tucson, 1995b.

Kaye, J. A., S. A. Penkett, and F. M Ormond, Report on concentrations, lifetimes, and trends of CFCs, halons, and related species, *NASA Ref. Publ.*, *1339*, 1994.

Kinnison, D. E., K. E. Grant, P. S. Connell, D. A. Rotman, and D. J. Wuebbles, The chemical and radiative effects of the Mount Pinatubo eruption, *J. Geophys. Res.*, *99*, 25,705–25,731, 1994.

Kumer, J. B., J. L. Mergenthaler, and A. E. Roche, CLAES CH_4, N_2O, and CCl_2F_2 (F12) global data, *Geophys. Res. Lett.*, *20*, 1239–1242, 1993.

Legrand, M. R., F. Stordal, I. S. A. Isaksen, and B. Rognerud, A model study of the stratospheric budget of odd nitrogen, including effects of solar cycle variations, *Tellus, Ser. B*, *41*, 413–426, 1989.

Lin, S.-J., and R. B. Rood, Multidimensional flux-form semi-Lagrangian transport schemes, *Mon. Weather Rev.*, *124*, 2046–2070, 1996.

Lindzen, R. S., Turbulence and stress owing to gravity wave and tidal breakdown, *J. Geophys. Res.*, *86*, 9707–9714, 1981.

Luo, M., R. J. Cicerone, J. M. Russell III, and T. Y. W. Huang, Observations of stratospheric hydrogen fluoride by Halogen Occultation Experiment (HALOE), *J. Geophys. Res.*, *99*, 16,691–16,705, 1994.

McCormick, M. P., Initial assessment of the stratospheric and climatic impact of the 1991 Mount Pinatubo eruption: Prologue, *Geophys. Res. Lett.*, *19*, 149, 1992.

McPeters, R. D., and G. J. Labow, An assessment of the accuracy of 14.5 years of Nimbus 7 TOMS version 7 ozone data by comparison with the Dobson network, *Geophys. Res. Lett.*, in press, 1996.

McPeters, R. D., et al., Nimbus-7 Total Ozone Mapping Spectrometer (TOMS) data products user's guide, *NASA Ref. Publ.*, *1384*, 1996a.

McPeters, R. D., S. M. Hollandsworth, L. G. Flynn, J. R. Herman, and C. J. Seftor, Long-term ozone trends derived from the 16.7-year combined Nimbus 7/TOMS version 7 record, *Geophys. Res. Lett.*, in press, 1996b.

Minschwaner, K., R. J. Salawitch, and M. B. McElroy, Absorption of solar radiation by O_2: Implications for O_3 and lifetimes of N_2O, $CFCl_3$, and CF_2Cl_2, *J. Geophys. Res.*, *98*, 10,543–10,561, 1993.

Montzka, S. A., J. H. Butler, R. C. Myers, T. M. Thompson, T. H. Swanson, A. D. Clarke, L. T. Lock, and J. W. Elkins, Decline in the tropospheric abundance of halogen from halocarbons: Implications for stratospheric ozone depletion, *Science*, *272*, 1318–1322, 1996.

Newell, R. E., J. W. Kidson, D. G. Vincent, and G. J. Boer, *The General Circulations of the Tropical Atmosphere*, vol. 2, chap. 7, MIT Press, Cambridge, Mass., 1974.

Nightingale, R. W., et al., Global CF_2Cl_2 measurements by UARS CLAES: Validation by correlative data and models, *J. Geophys. Res.*, *101*, 9711–9736, 1996.

Pitari, G., L. Ricciardulli, and G. Visconti, High-speed civil transport impact: Role of sulfate, nitric acid trihydrate, and ice aerosols studied with a two-dimensional model including aerosol physics, *J. Geophys. Res.*, *98*, 23,141–23,164, 1993.

Planet, W. G., A. J. Miller, J. J. DeLuisi, D. J. Hofmann, S. J. Oltmans, J. D. Wild, I. S. McDermid, R. D. McPeters, and B. J. Connor, Comparison of NOAA-11 SBUV/2 ozone vertical profiles with correlative measurements, *Geophys. Res. Lett.*, *23*, 293–296, 1996.

Porter, H. S., C. H. Jackman, and A. E. S. Green, Efficiencies for production of atomic nitrogen and oxygen by relativistic proton impact in air, *J. Chem. Phys.*, *65*, 154–167, 1976.

Prather, M. J., Numerical advection by conservation of second-order moments, *J. Geophys. Res.*, *91*, 6671–6681, 1986.

Prather, M. J., and E. E. Remsberg, The atmospheric effects of stratospheric aircraft: Report of the 1992 Models and Measurements Workshop, *NASA Ref. Publ.*, *1292*, vols. 1–3, 1993.

Randel, W. J., and R. R. Garcia, Application of a planetary wave breaking parameterization to stratospheric circulation statistics, *J. Atmos. Sci.*, *51*, 1157–1168, 1994.

Randel, W. J., B. A. Boville, J. C. Gille, P. L. Bailey, S. T. Massie, J. B. Kumer, J. L. Mergenthaler, and A. E. Roche, Simulation of stratospheric N_2O in the NCAR CCM2: Comparison with CLAES data and global budget analyses, *J. Atmos. Sci.*, *51*, 2834–2845, 1994.

Reid, G. C., S. Solomon, and R. R. Garcia, Response of the middle atmosphere to the solar proton events of August–December 1989, *Geophys. Res. Lett.*, *18*, 1019–1022, 1991.

Rodriguez, J. M., M. K. W. Ko, and N.-D. Sze, The role of heterogeneous conversion of N_2O_5 on sulphate aerosols in global ozone losses, *Nature*, *352*, 134–137, 1991.

Rosenfield, J. E., P. A. Newman, and M. R. Schoeberl, Computations of diabatic descent in the stratospheric polar vortex, *J. Geophys. Res.*, *99*, 16,677–16,689, 1994.

Russell, J. M., III, L. L. Gordley, J. H. Park, S. R. Drayson, W. D. Hesketh, R. J. Cicerone, A. F. Tuck, J. E. Frederick, J. E. Harries, and P. J. Crutzen, The halogen occultation experiment, *J. Geophys. Res.*, *98*, 10,777–10,797, 1993.

Russell, J. M., III, M. Luo, R. J. Cicerone, and L. E. Deaver, Satellite confirmation of the dominance of chlorofluorocarbons in the global stratospheric chlorine budget, *Nature*, *379*, 526–529, 1996a.

Russell, J. M., III, L. E. Deaver, M. Luo, R. J. Cicerone, J. H. Park, L. L. Gordley, G. C. Toon, M. R. Gunson, W. A. Traub, and R. Zander, Validation of hydrogen fluoride measurements made by HALOE experiment from the UARS platform, *J. Geophys. Res.*, *101*, 10,163–10,174, 1996b.

Schneider, H. R., M. K. W. Ko, C. A. Peterson, and E. R. Nash, Interannual variations of ozone: Interpretation of 4 years of satellite observations of total ozone, *J. Geophys. Res.*, *96*, 2889–2896, 1991.

Siskind, D. E., and J. M. Russell III, Coupling between middle and upper atmospheric NO: Constraints from HALOE observations, *Geophys. Res. Lett.*, *23*, 137–140, 1996.

Solomon, S., and R. R. Garcia, Transport of thermospheric NO to the upper stratosphere?, *Planet. Space Sci.*, *32*, 399–409, 1984.

Solomon, S., D. W. Rusch, J.-C. Gerard, G. C. Reid, and P. J. Crutzen, The effect of particle precipitation events on the neutral and ion chemistry of the middle atmosphere, 2, Odd hydrogen, *Planet. Space Sci.*, *29*, 885–892, 1981.

Solomon, S., R. W. Portmann, R. R. Garcia, L. W. Thomason, L. R. Poole, and M. P. McCormick, The role of aerosol variations in anthropogenic ozone depletion at northern midlatitudes, *J. Geophys. Res.*, *101*, 6713–6727, 1996.

Stolarski, R. S., P. Bloomfield, R. D. McPeters, and J. R. Herman, Total ozone trends deduced from Nimbus 7 TOMS data, *Geophys. Res. Lett.*, *18*, 1015–1018, 1991.

Stolarski, R. S., et al., Scientific assessment of the atmospheric effects of stratospheric aircraft, *NASA Ref. Pub. 1381*, 110 pp., 1995.

Tabazadeh, A., and R. P. Turco, A model for heterogeneous chemical processes on the surfaces of ice and nitric acid trihydrate particles, *J. Geophys. Res.*, *98*, 12,727–12,740, 1993.

Thomason, L. W., L. R. Poole, and T. Deshler, A global climatology of stratospheric aerosol surface area density deduced from Stratospheric Aerosol and Gas Experiment II measurements: 1984–1994, *J. Geophys. Res.*, in press, 1996.

Thorne, R. M., Energetic radiation belt electron precipitation: A natural depletion mechanism for stratospheric ozone, *Science*, *195*, 287–289, 1977.

Tie, X.-X., G. P. Brasseur, B. Briegleb, and C. Granier, Two-dimensional simulation of Pinatubo aerosol and its effect on stratospheric ozone, *J. Geophys. Res.*, *99*, 20,545–20,583, 1994.

Trepte, C. R., R. E. Veiga, and M. P. McCormick, The poleward dispersal of Mount Pinatubo volcanic aerosol, *J. Geophys. Res.*, *98*, 18,563–18,573, 1993.

Tung, K. K., and H. Yang, Dynamical component of seasonal and year-to-year changes in Antarctic and global ozone, *J. Geophys. Res.*, *93*, 12,537–12,559, 1988.

Turco, R. P., Photodissociation rates in the atmosphere below 100 km, *Geophys. Surv.*, *2*, 153–192, 1975.

Vitt, F. M., and C. H. Jackman, A comparison of sources of odd nitrogen production from 1974 through 1993 in the Earth's middle atmosphere as calculated using a two-dimensional model, *J. Geophys. Res.*, *101*, 6729–6739, 1996.

Wang, P.-H., P. Minnis, and G. K. Yue, Extinction coefficient (1 micron) properties of high-altitude clouds from solar occultation measurements (1985–1990): Evidence of volcanic aerosol effect, *J. Geophys. Res.*, *100*, 3181–3199, 1995.

Waters, J. W., et al., Validation of UARS Microwave Limb Sounder ClO measurements, *J. Geophys. Res.*, *101*, 10,091–10,127, 1996.

World Meteorological Organization (WMO), Scientific assessment of ozone depletion: 1991, *Rep. 25*, Global Ozone Res. and Monit. Proj., Geneva, 1991.

World Meteorological Organization (WMO), Scientific assessment of ozone depletion: 1994, *Rep. 37*, Global Ozone Res. and Monit. Proj., Geneva, 1995.

Zander, R., M. R. Gunson, J. C. Foster, C. P. Rinsland, and J. Namkung, Stratospheric $ClONO_2$, HCl, and HF concentration profiles derived from atmospheric trace molecule spectroscopy experiment Spacelab 3 observations: An update, *J. Geophys. Res.*, *95*, 20,519–20,525, 1990.

S. Chandra and C. H. Jackman, Laboratory for Atmospheres, Code 916, NASA Goddard Space Flight Center, Greenbelt, MD 20771. (e-mail: jackman@assess.gsfc.nasa.gov)

D. B. Considine and E. L. Fleming, Applied Research Corporation, 8201 Corporate Drive, Landover, MD 20785.

J. E. Rosenfield, General Sciences Corporation, 6100 Chevy Chase Drive, Laurel, MD 20707.

(Received May 9, 1996; revised September 20, 1996;
accepted October 3, 1996.)